JOURNAL OF MATERIALS SCIENCE 9 (1974) 1104–1114

In-situ observations of the annealing of liquid lead inclusions entrained in an aluminium matrix

M. McLEAN, M. S. LOVEDAY
Division of Inorganic and Metallic Structure, National Physical Laboratory, Teddington, Middlesex, UK

The changes in configuration of cylindrical inclusions of molten lead entrained in an aluminium matrix have been observed *in-situ* using hot-stage high voltage electron microscopy. Three distinct types of events were observed and analysed. The cylindrical inclusions spheroidized over a wide temperature range due to capillary forces; the resultant spherical inclusions migrated in the temperature gradient caused by electron beam heating; and impinging inclusions coalesced due to capillary forces.

The kinetics of the spheroidization and sintering events are controlled by the rate of diffusion of Al in liquid Pb and the data yield estimates for this diffusivity at various temperatures. The mechanism operating during thermal migration depends on the radius of the inclusion; volume diffusion kinetics control for the larger inclusions ($r > 0.8$ μm) and interface kinetics dominate the smaller inclusions ($r < 0.8$ μm).

1. Introduction

The presence of inclusions or a fibrous phase within a metallic matrix can lead to improvements in the mechanical properties, machinability or bearing characteristics of the material. However, at temperatures where significant mass transport can occur by diffusional processes, the morphology and size of inclusions entrained within a matrix can change thus altering these structure dependent properties. In recent years, many studies have been reported of the stability of such two-phase materials with respect to Ostwald ripening [1], spheroidization [2], the presence of temperature gradients [3] and intense gravitational fields [4]. However, *in-situ* observations have only been reported for systems which are transparent to visible [3] or infra-red [5] light and which can be examined by conventional optical microscopy. Thus Anthony and Cline have studied brine inclusions within KCl [3] and Jones and Chadwick [6] have examined certain organic compounds, one of which may be regarded as an analogue to metal alloys. Metallic systems have been studied by interrupting the heat-treatment and examining the inclusion configuration by a variety of techniques such as conventional metallography [19], microradiography [7], transmission [8] and scanning electron microscopy [9]. The latter approach has obvious disadvantages in interpretation since a statistical approach must be used in general rather than following the detailed changes of individual events. Previous *in-situ* experiments on transparent model systems have also been restricted by the resolution of the optical microscope.

In the present study aluminium foils, 8 to 10 μm thick, containing a fine dispersion of molten lead inclusions, 0.1 to 1 μm in diameter, have been examined using high voltage electron microscopy (HVEM) with hot stage facilities. The improved resolution over conventional optical microscopy and micro-radiography has permitted the examination of much smaller features where morphological changes by diffusional transport can be observed at significantly lower temperatures. Consequently, complementary information concerning the kinetics of mass transport, obtained by HVEM and microradiography [7], can be obtained over a wide temperature range. The Al—Pb system studied is typical of a wide range of structural metals where a soft phase is added in order to improve the bearing or machining properties of the material.

Three types of events have been observed and analysed during the present series of experiments. Initially the lead inclusions were cylindrical in shape and, on heating, these spheroidized under the influence of capillary forces. The rate of spheroidization was dependent on both the inclusion size and temperature and these data allow the identification and measurement of the operative mass transport mechanism following the procedures recently described by McLean [7]. After spheroidization the resulting spherical inclusions migrated towards the centre of the field of view under the influence of the temperature gradient imposed in the plane of the specimen due to electron beam heating. Such thermal gradient migration has been the subject of several recent studies because it gives rise to the distortion of certain nuclear fuel elements. By observing the relationship between inclusion size and velocity the operative mass transport mechanism can again be identified. When the migrating droplets impinged they merged into a single sphere thus reducing the total surface energy of the system. Nichols and Mullins [10] have described this phenomenon theoretically so that by carefully measuring the changes in shape of the collapsing spheres, the appropriate diffusivities can be calculated.

2. Experimental

The aluminium-lead alloys were prepared by inductively melting a mixture of 95% Al and 5% Pb by weight in an atmosphere of argon at about 1000° C. At this temperature there is considerable solubility of Pb in Al. The melt was then cast into a 25 mm diameter chilled copper mould when most of the lead precipitated into spherical globules due to the reduced solubility. The ingot was swaged and portions retained after various deformations. During swaging the spherical inclusions were deformed into roughly cylindrical shapes, the cylinder axes being parallel to the axis of the rod.

Specimens were prepared by cutting thin sheets, $\sim$ 1 mm thick, from the rods so that the lead cylinders were parallel to the surface of the sheet. The material was thinned for observations in the electron microscope by mechanical abrasion until it was 30 μm thick and chemical thinning in a solution of phosphoric, nitric and sulphuric acids* until about 8 μm thick. This was loaded in a resistively heated furnace type heating cartridge in an AEI EM7 electron microscope. The lead inclusions were observed in transmission at 10^6 V and the image continuously recorded using a video unit as the temperature was increased. The recorded image was subsequently transferred to 16 mm film at a recorded speed of $16\frac{2}{3}$ frames per second for frame by frame analysis.

3. Spheroidization

3.1. Theory

In a recent study of the spheroidization of cylindrical lead inclusions in aluminium, McLean [7] has shown that there are two basic modes by which cylinders can spheroidize. When the aspect ratio of the inclusion is less than about 8 to 1 it will collapse to a single sphere of the same volume, whereas more elongated inclusions split into a series of smaller spheres.

The time τ for the first droplet to be detached from the end of a long cylindrical inclusion is related to the inclusion radius R_0 by the following proportionality

$$R_0^n \propto \tau \tag{1}$$

where the exponent n takes the values 1, 2, 3 or 4 depending on whether mass transport occurs by viscous flow, evaporation-condensation, volume diffusion or interface diffusion respectively. The constant of proportionality incorporates the relevant diffusivities, interfacial energies and geometrical constants. For the case, which is relevant to this study, where diffusion of the matrix material within the inclusion is rate controlling,

$$R_0^3 = 0.035\, B\tau \tag{2}$$

where

$$B = \frac{cD\gamma\Omega^2}{kT}\cdot \tag{3}$$

c is the equilibrium concentration of Al in liquid Pb; D is the diffusivity of Al in Pb; γ is the Al/Pb interfacial energy which is assumed to be isotropic; Ω is the atomic volume of Al and kT is the thermal energy.

In the case of the shorter collapsing cylinder, the rate of change in length $\mathrm{d}Z/\mathrm{d}t$ is given by

$$\frac{\mathrm{d}Z}{\mathrm{d}t} \propto \frac{t}{R_0^{n-1}} \tag{4}$$

where n has the same significance as in Equation

*90:25:25 parts by volume of orthophosphoric, nitric and sulphuric acids respectively.

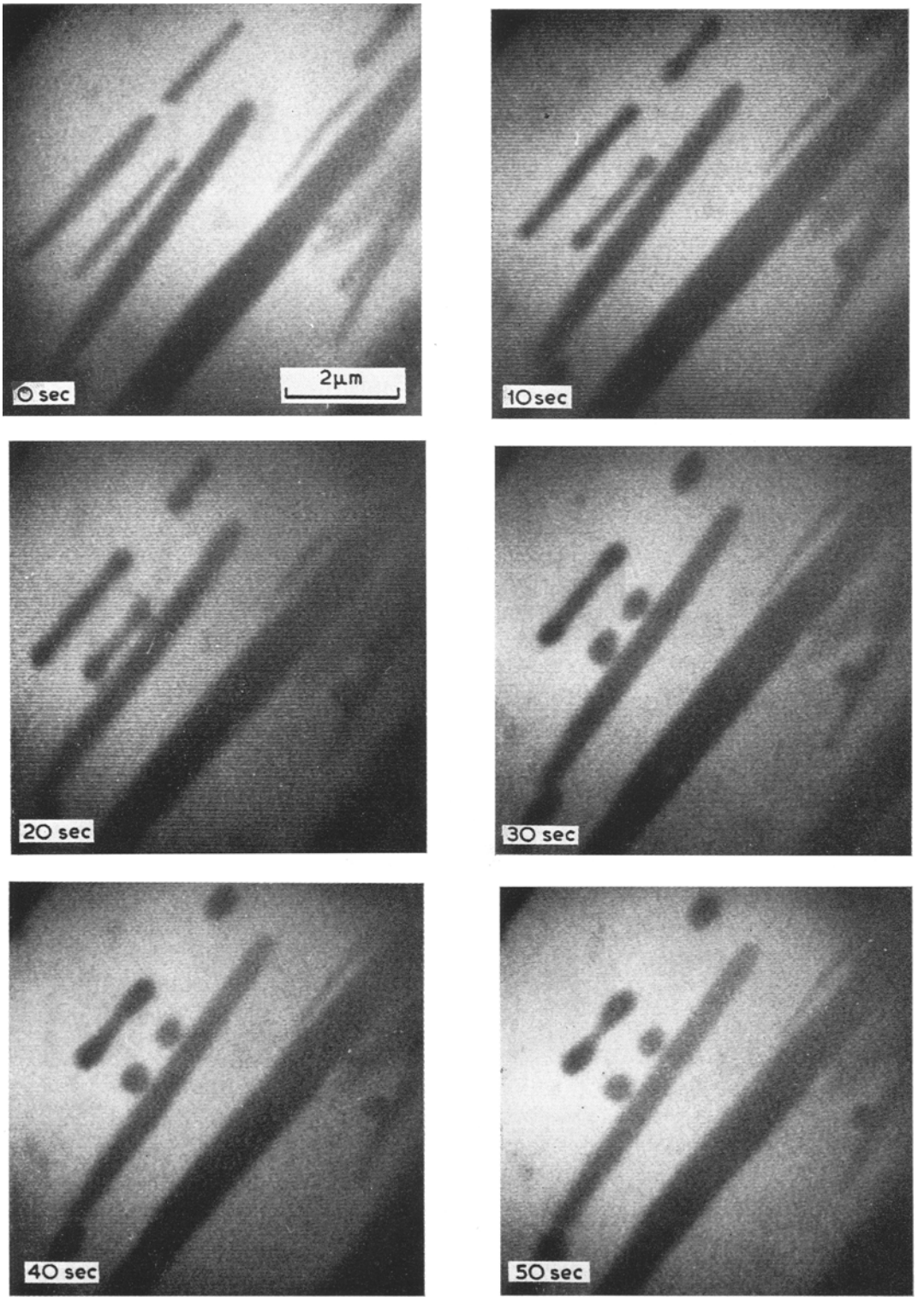

Figure 1 A typical sequence of electron micrographs, photographed from a video recording, showing the spheroidization of Pb cylinders in an Al matrix at 360°C. The interval between each micrograph is 10 sec.

1. Again for the case of diffusion within the inclusion being rate controlling

$$\frac{dZ}{dt} = -\frac{0.33B}{R_0^2} \quad (5)$$

where B is given by Equation 3.

Consequently, the operative mass transport mechanism can be identified by following the rate of spheroidization of inclusions of various sizes and the appropriate diffusivities determined at various temperatures.

3.2. Results

A typical sequence of micrographs is shown in Fig. 1 illustrating the two types of spheroidization discussed above. The smaller inclusions change in shape much more rapidly than the larger as would be expected. McLean [7] has previously demonstrated that spheroidization of larger inclusions in this system occurs by a volume diffusion mechanism, the diffusion of Al in liquid Pb being rate controlling. The present results are quite consistent with that finding, as evidenced by the constancy of the product $R_0^2(dZ/dt)$ at a fixed temperature. Some typical results, at 360°C, are listed in Table I.

TABLE I Rate of retraction, (dZ/dt), of the ends of cylinders of Pb of various radii, R_0, at 360°C.

R_0	$\frac{dZ}{dt}$	$R_0^2 \frac{dZ}{dt}$
(10^{-1} μm)	(10^{-2} μm sec^{-1})	(10^{-4} μm^3 sec^{-1})
1.60	0.5	1.28
1.40	0.7	1.40
1.30	0.7	1.20
1.20	1.0	1.40
0.75	2.2	1.20
0.70	2.0	0.98

Plots of the retraction of the ends of two inclusions are shown in Fig. 2 as a function of time. Inclusion P retracts initially at a uniform rate and eventually forms a single sphere; the gradient of this, and similar, curves may be substituted in Equation 5 to obtain a measure of the mobility B. Inclusion Q, however, forms a string of droplets with a characteristic detachment time τ of about 40 sec. Again B may be estimated from this information using Equation 2. The solid curve branches on drop detachment, the continuous curve showing the continuing relaxation of the drop relative to the origin, and the stepped branch showing the retraction of the parent inclusion. After detachment of the second droplet, the length of the parent rod was too short to allow further division.

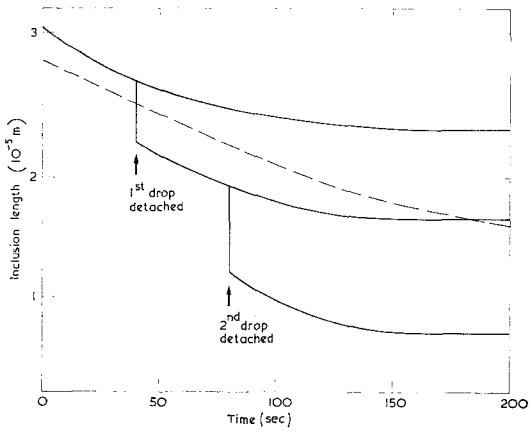

Figure 2 Plot of the retraction of the end of cylindrical inclusions as a function of time. The dashed curve refers to inclusion P which collapsed to a single sphere. The solid curve is for inclusion Q from which two droplets detached.

The values of B thus derived at various temperatures are plotted in Fig. 3 as a function of $1/T$. The results previously obtained by McLean [7] on larger inclusions using a microradiographic technique are included. The two sets of results are complementary, covering a wide temperature range, between the melting points of aluminium and lead.

3.3. Discussion

The data presented in Fig. 3 can be analysed to give an estimate of the diffusivity of aluminium in liquid lead, D. By combining the experimental values of B with McLean's [7] measurements of γ of 347 mJm^{-2} and Dardel's [11] estimates of c, D can be computed from Equation 3. This is shown in Fig. 4 as a plot of $\log D$ versus $1/T$. The values of D thus derived are critically dependent on the accuracy of the data on the solubility of Al in liquid Pb. The only-available data, due to Dardel, are some twenty-five years old and were obtained without the present sophisticated techniques. However, even assuming an error of ± 100%, our conclusions would not be seriously affected.

In a previous publication, McLean [7] concluded that the principal mode of spheroidization of fibres was associated with the retraction and detachment of the fibre ends rather than the spontaneous growth of periodic shape perturbations, as described by Rayleigh [12] for liquid

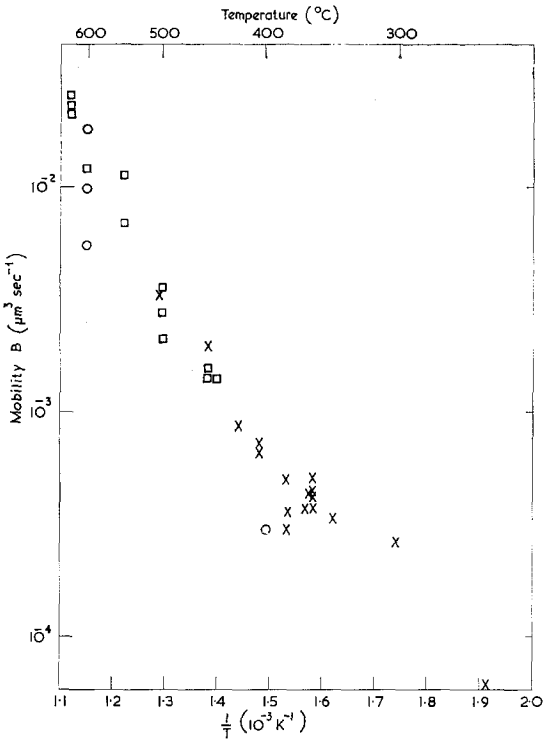

Figure 3 The variation of the mobility factor of Al in Pb, B, with temperature plotted as $\log_{10}$ B versus $1/T$. × – present spheroidization experiments; ○ – present sphere coalescence experiments; □ – spheroidization experiments using microradiography [7].

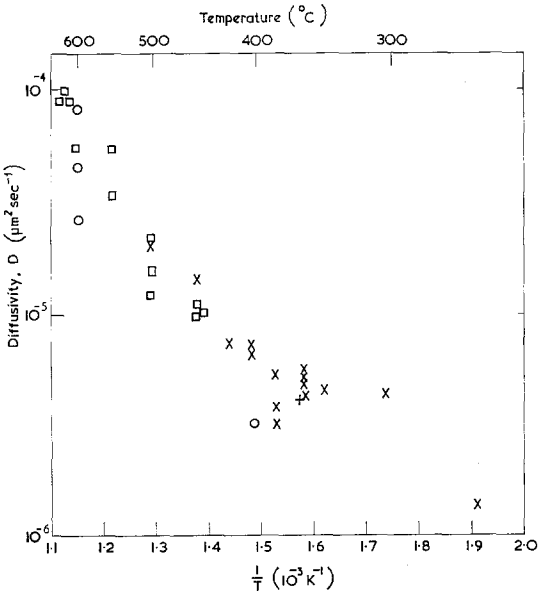

Figure 4 The variation of the diffusivity of Al in Pb, D, with temperature plotted as $\log_{10}$ D versus $1/T$. This has been computed from the data presented in Fig. 3.

jets. The present results confirm this view. Since the anisotropy of the Al/Pb interfacial energy is very small the conditions for Rayleigh mode spheroidization are more favourable than in, for example, directionally solidified composites where the fibres generally have low energy facets. In the latter case, any shape perturbation will involve the creation of high energy interfaces. This suggests that the drop detachment mode of fibre degradation, which initiates at the high energy cap at the fibre end, will always be dominant in faceted structures and consequently fibre length will control the life of fibre reinforced composites at elevated temperatures.

4. Thermal migration

4.1. Theory

The presence of a temperature gradient generates a concentration gradient within any material containing two or more components. This results from the variation of equilibrium solubilities with temperature. For the case under consideration, of liquid inclusions within a solid matrix, the matrix material diffuses in the liquid down the concentration and, hence, the temperature, gradient. The solid phase, therefore, dissolves at the hot end of the inclusion and condenses at the cool end with the result that the liquid inclusion migrates up the temperature gradient.

Shewmon [13] has shown that the mass transport mechanism can be identified from the variation of inclusion velocity with size for a fixed temperature gradient. As the inclusion size increases, the velocity either increases, is constant or decreases when the controlling mechanisms are interface kinetics, volume diffusion or interface diffusion, respectively. Tiller [14] has considered the case where there is competition between interface kinetics and volume diffusion control in more detail. His results, which qualitatively agree with Shewmon's predictions, indicate that the form of the size versus velocity variation significantly depends on the mechanism of dissolution at the solid-liquid interface. In the regime where diffusion within the liquid inclusion is rate controlling, the velocity of the inclusion, V, is given by

$$V = \frac{DG}{m(1-k)C} \tag{6}$$

where D is the diffusivity of the solid phase in the liquid; G is the local temperature gradient

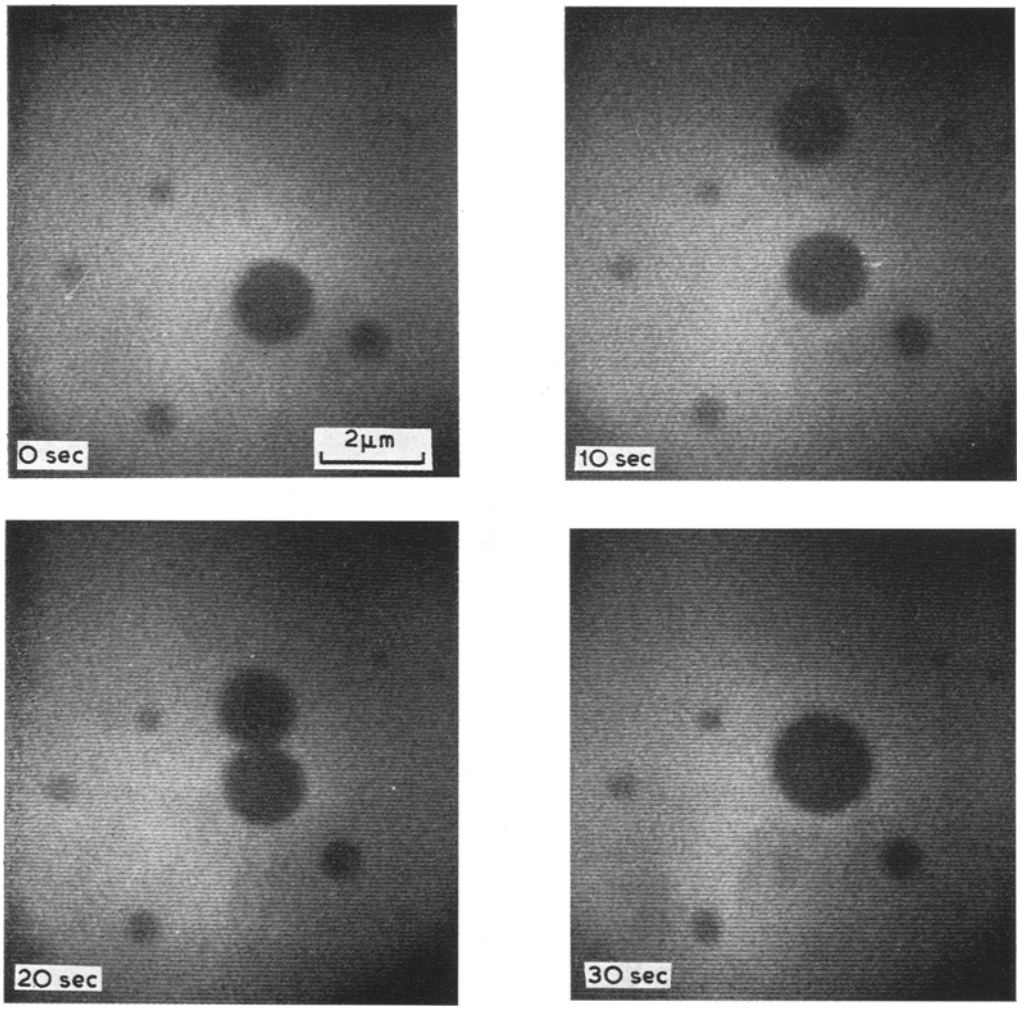

Figure 5 A typical sequence of electron micrographs at 10 sec intervals showing the thermal migration of Pb inclusions in Al at 597°C.

within the inclusion; m is the slope of the liquidus for the composition of inclusion; C and kC are the concentration of the solid component in the solid and liquid respectively.

Equation 6 should contain an additional term due to the Soret effect. The Soret coefficient, σ, expresses the difference due to the interaction between mass and heat flow between the actual concentration gradient and that predicted from equilibrium solubilities. An additional term should be included of the form

$$V = DG\left(\frac{1}{m(1-k)C} + \sigma\right). \qquad (7)$$

However, in the absence of a reliable estimate of σ, it will not be considered in the following analysis. This assumption is probably reasonable as judged from the relative contributions of the two terms in systems such as KCl [3]. Nevertheless our findings are subject to this uncertainty.

4.2. Results

Fig. 5 shows a typical sequence of electron micrographs at 10 sec intervals demonstrating the migration of lead inclusions at a nominal temperature of 597°C. The smallest inclusions show no measurable motion while the large inclusions migrate relatively rapidly. A plot of the dependence of inclusion velocity on inclusion radius is shown in Fig. 6 and three regimes are apparent. Inclusions less than 0.12 μm in radius show no measurable motion; for radii between

0.12 and 0.80 μm, the velocity increased steadily to a maximum value of 7.5×10^{-2} μm sec^{-1}; large inclusions (> 0.80 μm) had a constant velocity of 7.5×10^{-2} μm sec^{-1}. These observations were all made at constant setting of both the electron microscope and the heating cartridge in order to ensure that the temperature gradient remained constant.

4.3. Discussion

The present results, when interpreted in terms of Shewmon's predictions [13], clearly indicate a transition from interface reaction kinetics to volume diffusion control as the inclusion radius exceeds 0.80 μm. The lack of mobility of the smallest droplets ($r < 0.12$ μm) is less easily explained. Anthony and Cline [3] have proposed an activation barrier to dissolution at the solid-liquid interface which could lead to the effect. However, the results are also compatible with Tiller's predictions [14] when dissolution occurs by either a screw dislocation or a two dimensional nucleation mechanism. In these cases, the velocity approaches 0 parabolically with decreasing r.

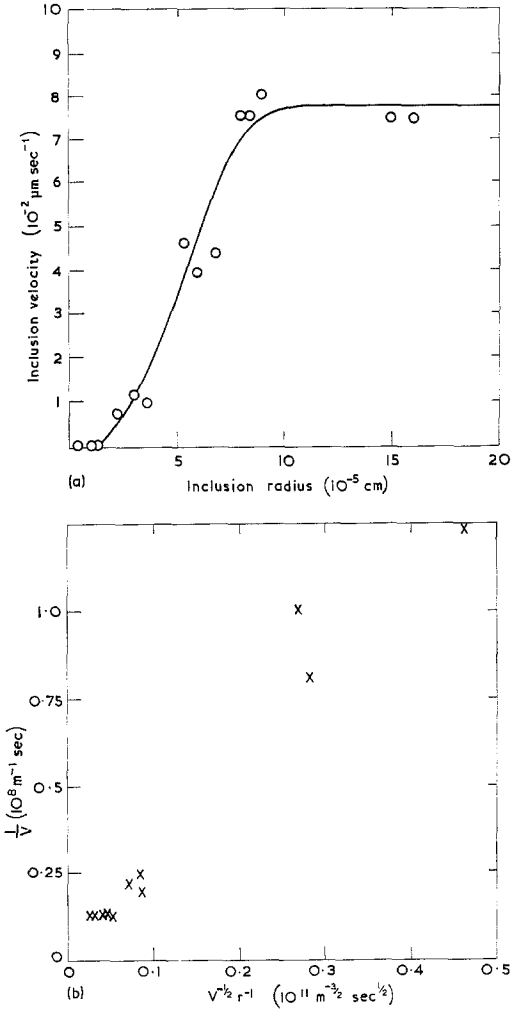

Figure 6 (a) The variation of inclusion velocity with inclusion radius at 597° C. (b) Data from (a) replotted as V^{-1} versus $V^{-\frac{1}{2}} r^{-1}$.

It is of interest to estimate the temperature gradients which are generated by electron beam heating using Equation 6. For the Al—Pb system $k \ll 1$; $mc = 1.2 \times 10^{3}$K [15]; $D = 5 \times 10^{3}$ μm^2 sec^{-1} [7]; and $V = 7.5 \times 10^{-2}$ μm sec^{-1}. Thus

$$G = 18.5 \times 10^{3} \text{ K m}^{-1}.$$

This local temperature gradient is related to the macroscopic temperature gradient G^* through the thermal conductivities of the two phases

$$G^* = \frac{2K_s + K_l}{3K_s} G$$

where K_s, K_l are the thermal conductivities of the solid and liquid phases respectively. For the Al/Pb specimen $K_l \ll K_s$ so that

$$G^* = 12.3 \times 10^{3} \text{ K m}^{-1}.$$

It is significant that the inclusions remain spherical during migration rather than elongating in the direction normal to the thermal gradient as predicted by Tiller [14] and observed experimentally by various authors [3, 6]. This indicates that in the competition between thermal gradient and surface energy forces, the latter dominates in establishing the shape of the inclusion. In Table II, the appropriate constants in Equation 7 are listed for the Al/Pb and KCl/brine systems together with the solid/liquid interfacial energy. It is clear that the relative contribution of surface energy in the Al/Pb system is dominant. It is unlikely that the unknown σ could be appreciably larger than in the KCl/brine case, since it would then significantly compete with the surface energy term in

TABLE II

	KCl/brine [3]	Al/Pb
Surface energy (mJm^{-2})	12	347
$G[m(1-k)C]^{-1}$ (m^{-1})	0.193×10^{-2}	0.154×10^{-2}
$G\sigma$ (m^{-1})	0.030×10^{-2}	?

controlling the shape of the inclusion. Consequently, our estimate of G is probably quite realistic.

Gale and Gosnold (private communication) have recently calculated the temperature distribution which should result from an axially symmetric incident beam with a radial current distribution: $I(r) = I_0 \exp(-r^2/a^2)$. They show that the maximum radial temperature gradient, which will apply over most of the beam, is given by

$$\left(\frac{dT}{dr}\right)_{max} \sim 0.31 \frac{H}{\pi a K} \frac{dE}{dt} \qquad (8)$$

where $H \equiv \pi a^2 I_0$ is the total beam current incident on the specimen; K is the thermal conductivity of the specimen; dE/dt is the average energy loss per electron passing through unit thickness of specimen and a is the radius of the electron beam. The appropriate constants in the present experiment are: $a = 5 \times 10^{-6}$ m and $K = 220$ J sec^{-1} K. dE/dt has been calculated using relativistic scattering theory and, for the case of aluminium irradiated by 1 MeV electrons, has a value of 6.4×10^{-11} J m^{-1}. During the experiment, a beam current of 10^{-8} A was measured after transmission through the specimen. Subsequent experiments using the same foil indicated that the beam was attenuated by a factor of between 20 and 50 during transmission. Inserting these values into Equation 8, a macroscopic temperature gradient G^* is predicted between the limits

$$7.1 \times 10^3 < G^* < 17.8 \times 10^3 \text{ K m}^{-1}.$$

The consistency of the estimates of G^* obtained from the thermal migration experiments and the electron beam calculations suggest that the initial neglect of the Soret coefficient is quite reasonable. The maximum value that σ can have is about 1.5×10^{-6} K^{-1} and a more realistic estimate is probably at least an order of magnitude less.

The temperature gradients deduced in the present study indicate that the absolute rise in temperature due to electron beam heating is quite small. Taking the grids of the copper mesh as a convenient heat sink (i.e. 100 μm square mesh) and assuming a constant temperature gradient, a rise in temperature of less than 1°C at the centre of the electron beam is predicted. This may be compared with the calculations of Fisher [16] who has computed the rise in temperature expected for various beam configurations. Our results are consistent with his predictions.

The data of Fig. 6a are replotted in Fig. 6b to show a linear relationship between V^{-1} and $V^{-\frac{1}{3}} r^{-1}$. This was predicted by Tiller [14] for the case where dissolution occurs by a screw dislocation mechanism and he derived the following relationship

$$V^{-1} = \frac{mC}{DG} + \frac{1}{2G\mu^{\frac{1}{3}}} V^{-\frac{1}{3}} r^{-1}$$

where μ is the kinetic coefficient. The value of $\mu = 0.09$ mm sec^{-1} K^{-2} derived from the present results is quite consistent with the theoretical estimate of 0.15 mm sec^{-1} K^{-2} for the dissolution of pure aluminium by a screw dislocation mechanism [14]. Moreover the lack of mobility of the smallest inclusions may occur when the inclusion diameter is less than the mean spacing of dislocations. Thus the present results strongly suggest that a screw dislocation dissolution mechanism is operative.

5. Coalescence of inclusions

5.1. Theory

The coalescence of two spheres, motivated by the minimization of surface energy, has been treated theoretically by a number of authors. The most rigorous treatment is probably that due to Nichols and Mullins [10] and Nichols [17] who show that during the final stages when the shape of the merged inclusions can be described as a perturbation to the final spherical shape of radius R_0

$$\delta(t) = \delta(0) \exp\left(-\frac{t}{\tau}\right) \qquad (9)$$

where δ is the amplitude of the spherical harmonic perturbation to the spherical shape of the inclusion and τ is the relaxation time for the process. They have derived expressions for τ when a variety of mass transport mechanisms are operative and show that it is inversely proportional to R_0^3 and R_0^4 when volume and surface diffusion mechanisms are respectively rate controlling. For the particular case of interest in the present study when the relevant diffusion path is within the inclusion

$$\tau_V = -\frac{8B}{R_0^3}. \qquad (10)$$

B has the same meaning as in Equation 3. Observations of the rate of sintering of two

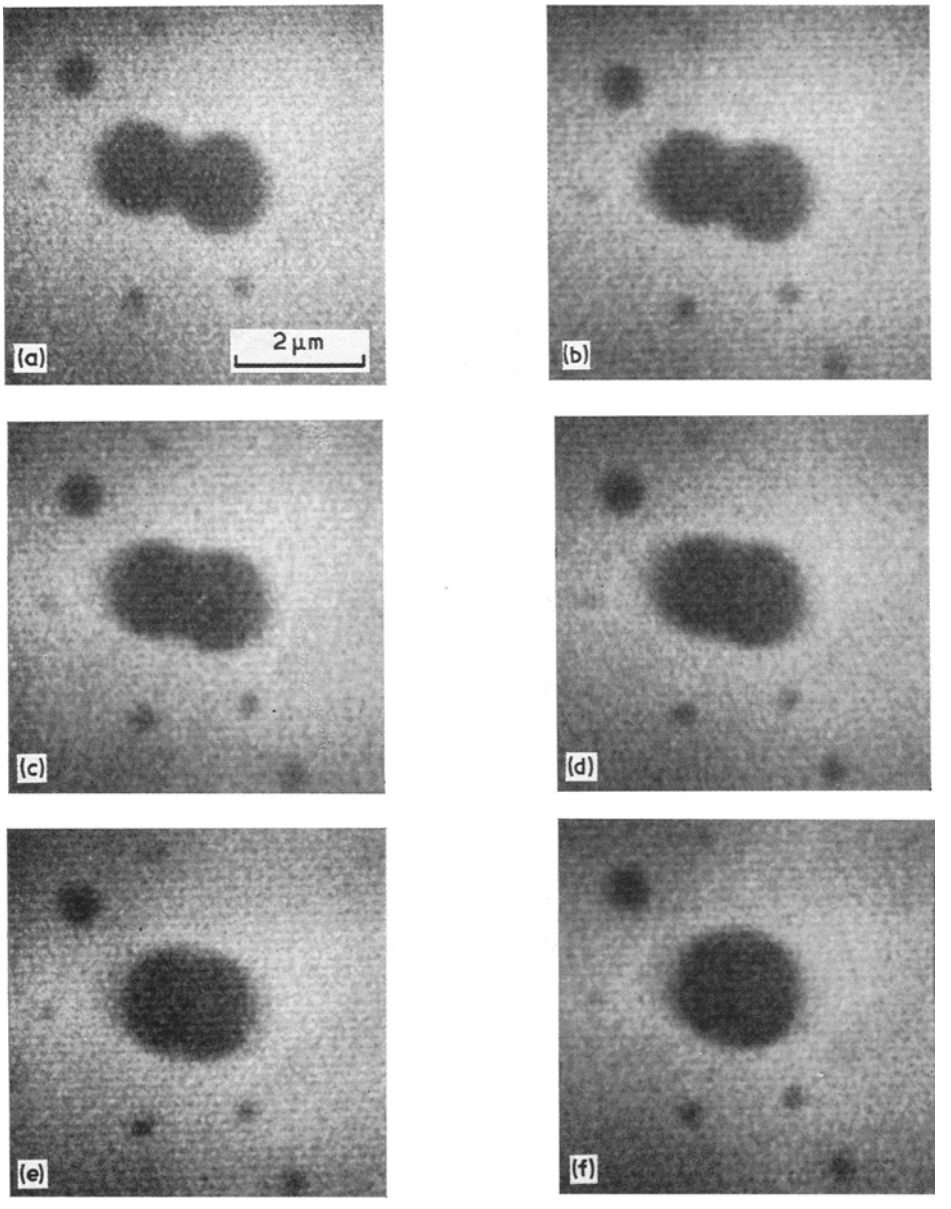

Figure 7 Sequential frames of a cine recording showing the coalescence of two spherical Pb inclusions at 597°C. The film speed is 16⅔ frames per second.

spherical inclusions can therefore provide an alternative measure of the mobility factor B.

5.2. Results

A sequence of successive frames of a cine recording of the coalescence of two spherical inclusions at 597°C is shown in Fig. 7. The deviation from spherical shape was characterised by the difference, Δ, between the final diameter and the inclusion length in the direction defined by the centres of the spheres and the initial point of contact; the change of Δ with time is shown in Fig. 8 as a plot of $\log_{10}\Delta$ versus t. The final slope of this graph may be identified with τ^{-1}.

Four such sintering events were recorded and analysed. The values of B derived are listed in Table III and included in Fig. 3 with the results derived from the spheroidization study.

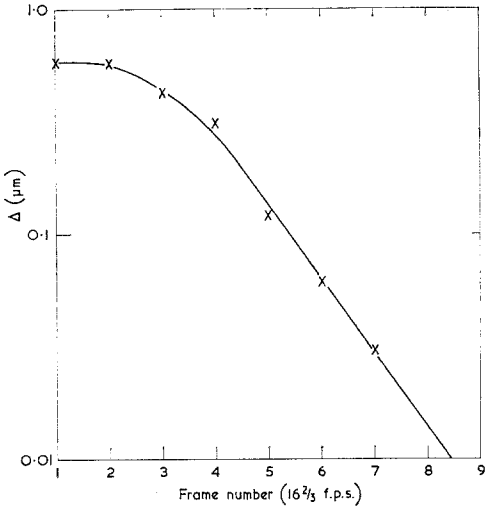

Figure 8 The collapse of two merging spheres with time, plotted as $\log_{10} \Delta$ versus film frame number. Δ is the difference between longest dimension and final diameter of the merging spheres. The film speed is 16⅔ frames per second.

TABLE III

B (m^3 sec^{-1})	Temperature (°C)
0.99×10^{-8}	597
0.55×10^{-8}	597
1.8×10^{-8}	597
3×10^{-10}	400

5.3. Discussion

The values of B derived from the above data are quite consistent with results of the spheroidization experiment presented in paragraph 3. This indicates that the geometrical parameters describing both events are quite compatible and probably realistic.

The coalescing sphere problem has previously been studied in the context of sintering of powder aggregates and there has been considerable debate concerning the relationship between particle size and rate of collapse of the spheres. The results presented above give support to the Nichols-Mullins analysis.

6. General discussion

6.1. Diffusion data

An important feature of our results is the apparent curvature of the Arrhenïus type plot shown in Fig. 4. This can either reflect inaccuracies in the data for the solubility of aluminium in lead which were used in calculating D, or it can be a real effect.The former explanation is more likely. The experimental errors in the solubility data are probably greatest at the highest temperatures, and this may account for the anomalously high activation energy of 72.7 kJ mol^{-1} which McLean [7] reported for diffusion of Al in Pb from data between 450 and 620°C. The present results would indicate a significantly lower value of about 25.6 kJ mol^{-1} at temperatures between 320 and 450°C. This is similar to other determinations of the activation energy for liquid state diffusion.

Only one spheroidization event was recorded where the lead was unambiguously solid. The value of D derived from this observation is significantly below the extrapolation of the liquid-state data indicating much slower diffusion in the solid as would be expected. The difference, however, is only about half an order of magnitude, rather than the two orders which are usually assumed to separate solid and liquid state diffusivities. This apparent anomaly may be due to the dominance of another mass transport mechanism, such as interfacial diffusion, rather than solid state volume diffusion.

6.2. Anisotropy of interfacial energy

The spherical shape of the inclusions after spheroidization clearly point to a low anisotropy of Al/Pb interfacial energy. The most significant observation on this subject is the retention of the spherical shape during thermal migration where a shape distortion is predicted and has been observed on several systems. Moreover the observations made have been directly made at the relevant temperature, so that there are no ambiguities due to cooling and observing the inclusions at room temperature. Thackery and Nelson [18], however, have observed quite anisotropic Pb inclusions in Al and have attributed this to a high anisotropy of solid Al/liquid Pb interfacial energy. As previously discussed by McLean [7], this apparent discrepancy is probably due to either shape changes during quenching to room temperature for observation, or to the development of a non-equilibrium growth form during the bombardment of Al by Pb^+ ions which was the method of introducing the inclusions.

6.3. Metallurgical applications

Soft metallic inclusions such as lead, tin, cadmium etc, are often introduced into structural metals such as steel, copper or aluminium in order to improve the bearing characteristics or

the machinability. In both cases it is suspected that the inclusion size distribution and shape significantly affect the efficiency of the alloys. Consequently, it may be desirable to control the form of the soft phase during the production of the materials. By means of a predetermined mechanical deformation followed by a spheroidizing heat-treatment the resultant inclusion form can be controlled within quite wide limits. Moreover, from a knowledge of the spheroidisation kinetics, the optimum heat treatment can easily be specified. Similarly an indication of the conditions which can be tolerated without spheroidization occurring may be relevant to the high temperature use of structures such as fibre reinforced composite materials.

References

1. A. J. ARDELL, *Metall. Trans.* **1** (1970) 525.
2. C. F. YEN and R. L. COBLE, *J. Amer. Ceram. Soc.* **55** (1972) 507.
3. T. R. ANTHONY and H. E. CLINE, *J. Appl. Phys.* **42** (1971) 3380.
4. *Idem, Phil. Mag.* **22** (1970) 893.
5. H. E. CLINE and T. R. ANTHONY, *J. Appl. Phys.* **43** (1972) 4391.
6. D. R. H. JONES and G. A. CHADWICK, *Phil. Mag.* **24** (1971) 1327.
7. M. MCLEAN, *Phil. Mag.* **27** (1973) 1253.
8. P. K. RASTOGI and A. J. ARDELL, *Acta. Met.* **19** (1971) 321.
9. J. L. WALTER and H. E. CLINE, *Metall. Trans.* **4** (1973) 33.
10. F. A. NICHOLS and W. W. MULLINS, *Trans. Met. Soc. AIME* **233** (1965) 1840.
11. Y. DARDEL, *Light Metals* **9** (1946) 220; *Z. Metallk.* **39** (1948) 214.
12. LORD RAYLEIGH, *Proc. Lond. Math. Soc.* **10** (1878) 4.
13. P. G. SHEWMON, *Trans. Met. Soc. AIME* **230** (1964) 1134.
14. W. A. TILLER, *J. Appl. Phys.* **34** (1963) 2757.
15. M. HANSEN, "Constitution of Binary Alloys" (McGraw-Hill, New York, 1958).
16. S. B. FISHER, *Radiation effects* **5** (1970) 239.
17. F. A. NICHOLS, *J. Appl. Phys.* **37** (1966) 2805.
18. P. A. THACKERY and R. S. NELSON, *Phil. Mag.* **19** (1969) 169.
19. M. F. ASHBY and R. M. A. CENTAMORE, *Acta. Met.* **16** (1968) 1081.

Received 27 November 1973 and accepted 16 January 1974.